The electrocatalytic oxidation of ethanol studied on a molecular scale

Lai, S.S.S.

CHAPTER 6

ETHANOL ELECTRO-OXIDATION ON PLATINUM IN ALKALINE MEDIA

The electrochemical oxidation of ethanol as well as its irreversible adsorption on platinum single-crystal electrodes has been studied in an alkaline solution. In addition, the adsorbed species in the ethanol oxidation reaction were also studied by means of surface enhanced Raman spectroscopy (SERS) on a platinum film electrode. It was found that the oxidation of ethanol is very sensitive to the electrode surface structure: a higher concentration of low-coordination sites increases the current, lowers the overpotential required and lowers the deactivation rate. Furthermore, the terrace length also affects the amounts and the nature of the adsorbed species: on Pt (110), only CO_{ad} was observed, whereas adsorbed CH_x could only be found on electrode surfaces with (111) terrace sites. Based on the results here, a model for the ethanol electro-oxidation reaction in alkaline media is presented, and the differences with the same reaction in acidic media are pointed out.

The contents of this chapter have been published: S. C. S. Lai and M. T. M. Koper, *Phys. Chem. Chem. Phys.*, **2009**, *11*, 10446-10456.

6.1 Introduction

The electrochemical oxidation of hydrogen and small organic molecules is a subject that has been studied extensively in the last decades in the context of utilizing these reactions in low temperature fuel cells [1]. In particular, the oxidation of ethanol has been the topic of numerous research papers [2-19]. This attention has mainly arisen due to the high energy density and the fact that ethanol is considered a 'green' chemical in the sense that it can be produced in large quantities as a renewable biofuel from the fermentation of biomass, and that both ethanol and its final oxidation product, carbon dioxide, are relatively non-toxic. In addition, the electro-oxidation of ethanol is also of academic interest, since it is, together with acetaldehyde, the smallest oxygenated organic molecule containing a carbon-carbon bond which needs to be broken to achieve full oxidation.

Since platinum is generally considered the best monometallic catalyst for the oxidation of small organic molecules, most studies have focused on ethanol oxidation on platinum in an acidic electrolyte for elucidating the reaction mechanism and identifying the intermediates and products [2-11]. It is generally accepted that the oxidation of ethanol proceeds via a dual pathway mechanism as shown in Scheme 6.1 [6, 7, 9, 10]: Ethanol can be oxidized to acetaldehyde and subsequently to acetic acid, transferring only 4 electrons in the process. Acetic acid marks a 'dead end' in the mechanism, since its further oxidation is very difficult under ambient conditions [9, 20]. Alternatively, the carbon-carbon bond can be cleaved in ethanol or acetaldehyde, yielding the adsorbed single carbon species CO_{ad} [4-8] and $CH_{(x)ad}$ (with $x = 1$ in acidic media) [5, 6]. These species can subsequently be oxidized to CO_2, liberating 12 electrons in total. Although this is the preferred pathway from a fuel cell application point of view, the single carbon adsorbates require a high overpotential to be oxidized [2,9], thereby reducing the efficiency of the reaction. In acidic media, it is found that the main current producing pathway for ethanol concentrations which would be of interest in direct ethanol fuel cells, is the C_2-pathway to acetaldehyde and acetic acid, while CO_2 formation only has a minor contribution [2-4]. In order to increase the activity of the ethanol oxidation reaction at low overpotentials as well as to increase the selectivity towards CO_2, bi- and trimetallic systems have been investigated extensively [12-18]. Nonetheless, the amount of CO_2 produced

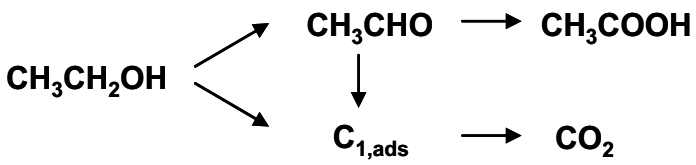

Scheme 6.1: *Schematic representation of the "dual pathway" mechanism for the electrocatalytic oxidation of ethanol.*

compared to acetaldehyde and acetic acid generally remains relatively low in acidic media.

The ethanol oxidation reaction in alkaline media has been much less studied, mainly due to the impracticalities that lie in the utilization of alkaline fuel cells [21-23]. One important issue is that an alkaline electrolyte is prone to progressive carbonation due to CO_2 retention, deactivating the electrolyte over time. In addition, proper alkaline membranes that are stable under fuel cell conditions over extended periods of time have been unavailable for a long time. However, as new solid alkaline electrolytes [24, 25] are being developed and new concepts, such as electrolyte recirculation [26] and the use of carbonate electrolyte [27], which will eject dissolved CO_2, are being tested, a renewed interest in alkaline fuel cell catalysis is warranted since it offers several considerable advantages compared to acidic electrolytes. From a material point of view, the range of electrode materials that is stable and could be employed in an alkaline environment is much wider, and therefore cheaper and less noble metals could be considered [28, 29]. From a fundamental point of view, it is often found that the electrocatalytic activity for the oxidation of organic fuels is larger in alkaline media in comparison with acidic media [30, 31]. An interesting example is the oxidation of carbon monoxide, a well studied model reaction as well as an intermediate in the complete oxidation of ethanol. Interestingly, the oxidation of CO in alkaline media occurs at smaller overpotentials compared to acidic media [32, 33], even on the reversible hydrogen electrode (RHE) scale, which should correct for 'trivial' pH effects. In addition, in the case of the ethanol oxidation reaction, it has been found that changing electrolyte pH also changes the product distribution. Employing differential electrochemical mass spectrometry (DEMS), Rao *et al*. found that in an alkaline membrane electrode assembly, the contribution of CO_2

to the total currents is about 55%, compared to 2% in acidic membrane electrode assembly [34].

Despite the clear advantages of employing an alkaline electrolyte for the ethanol oxidation reaction, there is still no clear mechanistic understanding of the reaction in alkaline media. In this work, we address this issue by studying the effect of the surface structure of the electrode on the reaction. In addition, we study the role of surface species in the oxidation mechanism with surface enhanced Raman spectroscopy.

6.2 Experimental

The electro-oxidation of ethanol on platinum has been studied in 0.1 M NaOH solutions. The solutions were prepared from NaOH pellets (Sigma Aldrich, 99.998%), ethanol (Merck, "Emprove") or deuterated ethanol (ethanol-d_6, 99%, Cambridge Isotope Laboratories) and ultra-pure water (Millipore MilliQ A10 gradient, 18.2 MΩ cm, 2-4 ppb total organic content). Argon (Hoekloos, purity 6.0) was purged through a 4 M KOH (Merck, pro analysi) solution prior to entering the electrochemical cell and used to deoxygenate all solutions.

The working electrodes used in this study for the voltammetric measurements were platinum bead-type single-crystal electrodes of Pt [n(111)×(111)] (or, equivalently, Pt [(n-1)(111)×(110)]) orientation . The surfaces studied were Pt (15 15 14) with n = 30, Pt (554) with n = 10, Pt (553) with n = 5 and the limiting cases Pt (111) and Pt (110), which were prepared according to Clavilier's method [35]. Prior to each experiment, the electrodes were flame-annealed and cooled down to room temperature in an argon (Hoekloos, purity 6.0) - hydrogen mixture (Hoekloos, purity 6.0) (*ca.* 3:1), after which they were transferred to the electrochemical cell under the protection of a droplet of deoxygenated ultra-pure water [36]. Voltammetric measurements were recorded on a computer-controlled Autolab PGSTAT 12 potentiostat (Ecochemie).

Surface enhanced Raman spectroscopic (SERS) measurements were performed with a HR 800 spectrograph (Jobin Yvon) with a holographic grating of 600 gr mm^{-1}. The confocal hole of the system was set at 100 μm. A CCD camera with 1024 × 256 pixels was used as detector. The excitation line was provided by a

20 mW HeNe laser at 632.8 nm. The laser beam was focused through an Olympus 50× microscope objective, which was not immersed in the electrolyte, into a 5 μm spot on the electrode surface. A notch filter was used to filter the SERS signal before reaching the sample. With this configuration, a resolution of 1.2 cm^{-1} was obtained.

The working electrode in the SERS experiments was a gold disk of 5 mm in diameter embedded in a PTFE shroud, which was mechanically polished with alumina (down to 0.3 μm), rinsed and treated ultrasonically in ultra-pure water before use. The gold electrode was roughened by applying a succession of 25 potential sweep oxidation and reduction cycles in 0.1 M KCl (Merck, pro analysis) from 1.25 V to -0.25 V vs. the Hg/Hg_2Cl_2 electrode [37]. An ultrathin film of a few monolayers of platinum [38] was deposited galvanostatically on the gold substrate from a 0.005 M H_2PtCl_6 (Sigma-Aldrich, ACS reagent) in 0.5 M Na_2HPO_4 (Merck, pro analysis) aqueous solution by applying a current of 0.4 mA cm^{-2} for 40 s [38]. In the SERS experiments, an IviumStat Potentiostat (Ivium Technologies) was used for potential control.

6.3 Results and discussion

6.3.1 Voltammetric studies

Figure 6.1 shows typical voltammetric profiles obtained for the electro-oxidation of ethanol in 0.1 M NaOH and 0.1 M $HClO_4$ on polycrystalline platinum. Both electrolytes show the typical profile for the oxidation of small organic molecules on a platinum electrode [39]: in the anodic sweep, the currents in the hydrogen underpotential deposition region (0.07 - 0.40 V) are suppressed due to surface blocking by decomposition products. Starting at 0.4 - 0.5 V, the adsorbed decomposition products are oxidized, liberating surface sites for continuous oxidation. At higher potentials, surface oxidation takes place, blocking adsorption of the reactant and causing the oxidation currents to decrease again. In the cathodic sweep, the surface oxides are reduced, reactivating oxidation currents until the potential is too negative to oxidize the adsorbed species and the surface is blocked again. Although the shapes of the voltammetric profiles are similar for both electrolyte solutions, there are some significant differences.

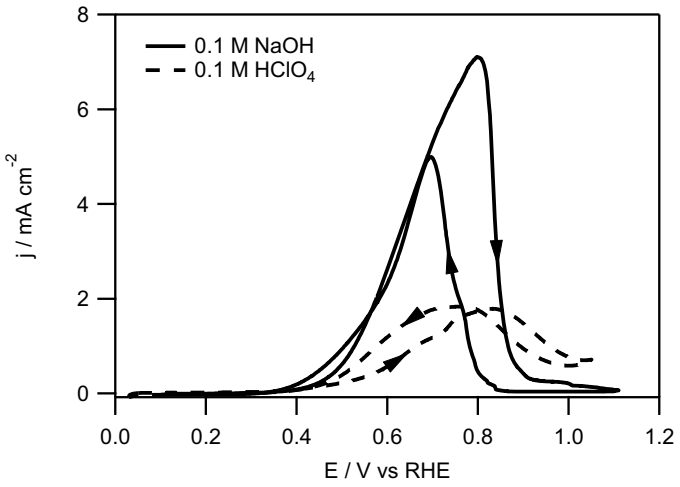

Figure 6.1: *Cyclic voltammograms (first cycles) for the electro-oxidation of 0.5 M ethanol in 0.1 M NaOH (solid line) and 0.1 M $HClO_4$ (dashed line) on polycrystalline platinum. The voltammograms were recorded at 10 mV s^{-1}. The arrows indicate the scan direction.*

First, the activity in sodium hydroxide solution is considerably enhanced compared to a perchloric acid solution (for which anion adsorption effects can be neglected). Second, there is a negative shift in the onset potential of the reaction of about 100 mV and in the peak potential of about 50 mV. Similar negative shifts have been found earlier for the oxidation of CO [40] and methanol [41, 42] and have been ascribed to a higher affinity of OH for low-coordinated step and defect sites. However, such 'trivial' pH effects should be accounted for by referring to the reversible hydrogen electrode. Third, it can be seen that the hysteresis between the positive and negative scan differs from that observed in acidic media. Although there is still a significant hysteresis related to the irreversibility of the surface oxidation reaction (above *ca.* 0.65 V), the hysteresis below *ca.* 0.65 V is almost absent in alkaline media. Since the size of the hysteresis loop below *ca.* 0.65 V is a measure for the difference in the processes in the anodic and cathodic scan, it is often related to the poisoning of the surface by strongly adsorbed intermediates [7]. This can be rationalized as follows: Since the coverage of oxidizable surface species in the anodic sweep (starting a low potentials with a high coverage) is different from the coverage in the cathodic sweep (starting at high potentials with a low coverage), the oxidation of surface

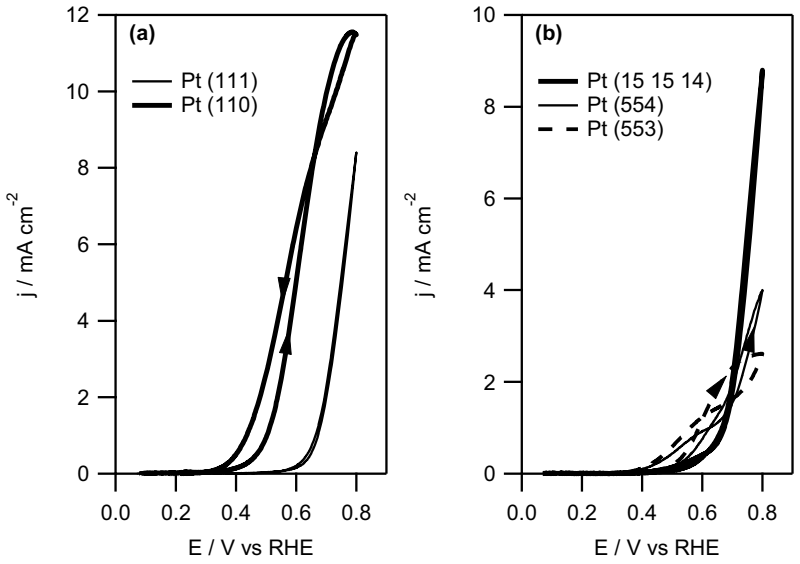

Figure 6.2: *Cyclic voltammograms (first cycles) for the oxidation of 0.5 M ethanol in 0.1 M NaOH on (a) Pt (111) and Pt (110), and (b) Pt (15 15 14), Pt (554) and Pt (553) at a scan rate of 10 mV* s^{-1}.

species is necessarily dependent on the sweep direction and must give rise to a hysteresis loop. The lack of hysteresis in this potential region between the anodic and cathodic sweep in the ethanol oxidation reaction in alkaline media suggests that the oxidation of adsorbed species does not play a significant role. This might imply that in alkaline media, no strongly adsorbed species are formed. Alternatively, it could also mean that surface species are formed, but these species are stable within the potential range, or that the oxidation of these species is sluggish and therefore only has a minor contribution to the total currents. We also note that a significant part of the current must be due to the formation of acetate, which presumably does not involve strongly adsorbed intermediates.

In order to obtain more insight into the origin of this remarkable activity in alkaline media, the ethanol oxidation reaction was performed on a series of platinum single-crystal electrodes in a sodium hydroxide solution. Similar experiments in acidic media have been described in detail in Chapter 3. The first

voltammetric cycles in sodium hydroxide electrolyte solution, sweeping between 0.07 V and 0.80 V, are shown in Figure 6.2. The positive potential limit was chosen before the onset of surface oxidation to avoid surface disordering due to the formation and subsequent reduction of irreversible surface oxides. It can be seen that the currents are monotonously increasing with increasing potential and the hysteresis between the positive and negative scans are minimal for Pt (111) and Pt (15 15 14), *i.e.* the surfaces with very wide terraces. Assuming that the current is primarily reflecting the C_2-pathway (the formation of acetaldehyde and/or acetate), this could suggest that poisoning through (strongly) adsorbed species is minimal on these surfaces, either due to a slower formation of adsorbates or facile removal of the adsorbates. Alternatively, in the other extreme, it could also suggest that adsorbate removal is very sluggish. Different voltammetric profiles can be found for Pt (110) and Pt (553). On these surfaces the currents peak a bit below the upper potential limit, and a small hysteresis can be observed, suggesting that surface adsorbed species do have an effect on the oxidation currents. Between these extremes, Pt (554), which has 10-atom wide terraces, shows intermediate behavior.

In addition to the differences in the general shape of the voltammetric curves, a structural effect can also be observed in the onset potentials of the reaction and in the total currents. It can be seen that the onset potential decreases with increasing step density: starting at Pt (111), the onset potential of the reaction shifts about 100 mV negatively when introducing steps. Increasing the amount of steps, while keeping terraces of (111)-orientation, further lowers the onset potential, although the effect is relatively small compared to the shift gained from Pt (111) to Pt (15 15 14), emphasizing the important effect of only a small amount of low-coordination sites. Finally, going from the stepped surfaces to Pt (110) leads to another decrease in the overpotential by *ca.* 100 mV. Therefore, at 'low' overpotentials (up to 0.70 V), the activity increases with decreasing terrace length. At high overpotentials, on the other hand, this trend is reversed. At potentials above 0.70 V, the currents generally decrease with increasing step density. Although the initial effect of introducing steps is relatively small as can be seen in the currents on Pt (111) and Pt (15 15 14), further decreasing the terrace length significantly inhibits the total activity at these high potentials. The notable exception for this trend is Pt (110), a surface which contains no (111) terrace sites, yet shows the highest activity over the entire potential range.

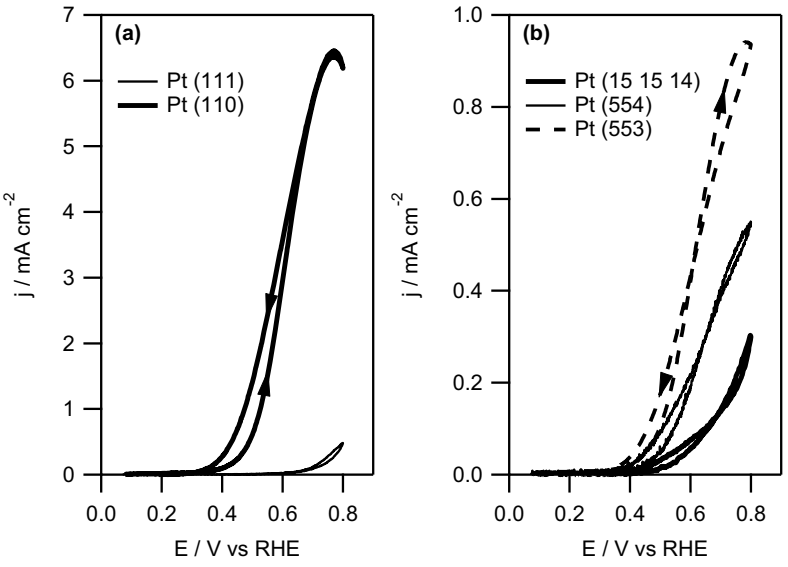

Figure 6.3: *Cyclic voltammograms (20th cycles) for the oxidation of 0.5 M ethanol in 0.1 M NaOH on (a) Pt (111) and Pt (110), and (b) Pt (15 15 14), Pt (554) and Pt (553) at a scan rate of 10 mV* s^{-1}.

Although the initial activity seems promising, it is also important to study the stability of the system. Therefore, cyclic voltammograms were recorded repeatedly until a 'stable' voltammogram was obtained. For all surfaces, the activity initially decreased rapidly with the number of voltammetric sweeps before it roughly stabilizes between the tenth and fifteenth voltammetric cycle. Upon further cycling, only small changes between subsequent scans were observed. To compare the stable voltammograms recorded on the different electrodes, Figure 6.3 shows the twentieth voltammetric cycles of ethanol oxidation in 0.1 M sodium hydroxide solution. In comparison with the first voltammetric cycles (Figure 6.2), a clear deactivation can be seen for all the surfaces. This deactivation may be due to several reasons [22], such as the depletion of the reactant species, structural surface modification due to repeated surface oxidation and reduction, structural surface modification induced by adsorbed species, or poisoning of the electrode surface by intermediates or contaminations. Due to the small surface area of the electrode, the consumption of ethanol is at most in the order of micromoles, which is negligible considering

the high initial concentration of ethanol. In addition, it is unlikely that the main cause of the deactivation is a depletion of the diffusion layer near the electrode (which would be related to the reaction rate and therefore to the measured currents), since the most active surface shows the lowest deactivation rate (*vide infra*). Surface modification due to repeated oxidation-reduction cycles should also be minimal, since the upper potential limit was chosen below the onset of (irreversible) surface oxidation. Furthermore, there is no indication for deactivation due to adsorbate induced reconstruction: the surfaces are suggested to be stable within this potential window [43], the general shape of the voltammogram does not change during deactivation and the H_{UPD} region is not changed after adsorbate stripping with respect to the blank voltammogram (*vide infra*), although it could be argued that any adsorbate induced reconstruction could be lifted after stripping of the adsorbate. Therefore, we propose that the main cause of the deactivation upon repeated cycling is surface poisoning by reaction intermediates, which is also supported by the fact that the amount of adsorbed hydrogen also decreases with the number of voltammetric sweeps. This issue will be further elaborated in the General Discussion section.

Although all surfaces lose activity upon repeated cycling, the rate of poisoning differs per surface. The highest activity was found for Pt (110), and the activity decreases with increasing terrace length, with the lowest activity for Pt (111) for all potentials. It should also be noted that this trend differs from the first voltammetric activity. In the first voltammogram, the relative activities of the different electrode surfaces was potential dependent, increasing with increasing step density at low potentials and decreasing with increasing step density at high potentials, with Pt (110) being the most active over the entire potential range. This change in the trend implies that the surface poisoning rate is also structure dependent. This is illustrated more clearly in Figure 6.4, which shows the ratio of the currents measured at 0.60 V and 0.70 V in the anodic sweep of the first voltammetric cycle and the twentieth voltammetric cycle. Both potentials show that the current density decrease is strongly dependent on the step density of the surface, suggesting that terraces are especially prone to poisoning. This effect is the largest for Pt (111), which shows only 5 - 10% of the initial activity in the stable cycles. On the other end of the spectrum, Pt (110) still retained over 50% of the initial activity. This behavior is remarkable, as normally the surface with the highest initial activity also exhibits the highest deactivation rate [44].

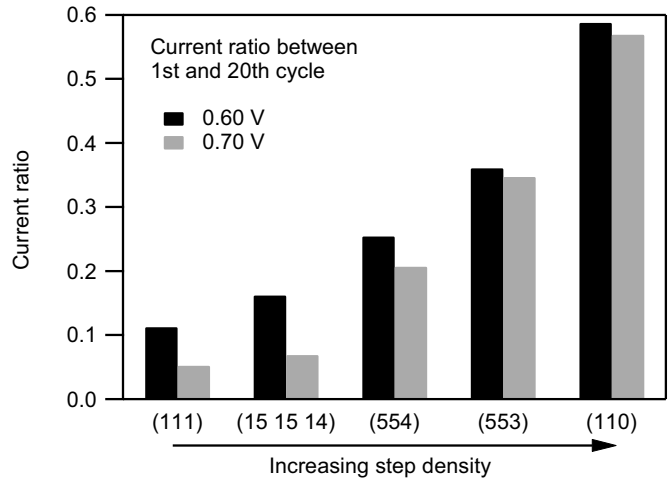

Figure 6.4: *Ratio of the currents at 0.60 V and 0.70 V of the positive-going scan of the first and the twentieth voltammetric cycles for the oxidation of ethanol.*

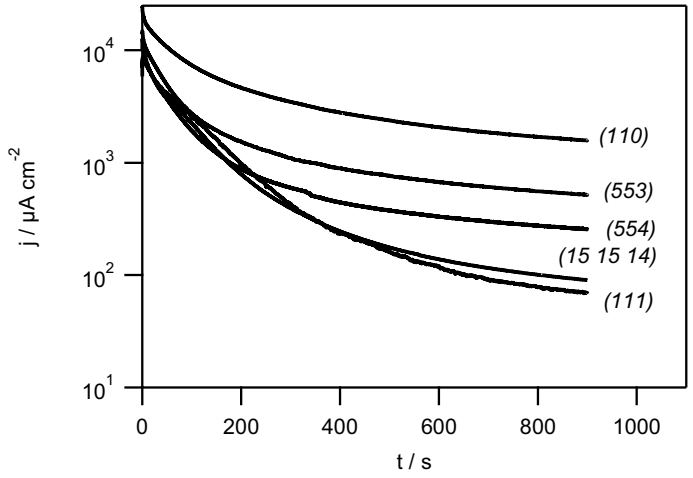

Figure 6.5: *Current-time transients for the oxidation 0.5 M ethanol in 0.1 M NaOH. The potential was stepped from 0.07 V to 0.70 V.*

The ethanol oxidation reaction was also studied over longer time-scales with potentiostatic measurements, as shown in Figure 6.5. In these measurements, the

potential was stepped from 0.07 V to 0.70 V at t = 0, after which the potential was kept constant for 15 minutes. The potential of 0.70 V was chosen because it was well in the potential region where all surfaces show oxidation currents. In addition, it is close to turning point in the effect of surface structure on the initial activity (*vide supra*). It can be seen that the final activity trend qualitatively mirrors the trend found in the voltammetric measurements. All surfaces show a monotonously decaying current over time, with the rate of decay being the lowest for Pt (110) and the highest for Pt (111). Furthermore, the final activity decreases with increasing terrace length. Finally, it should also be noted that the quantitative effect of the surface structure is very significant in alkaline media, with the most active surface showing an activity that is roughly two orders of magnitude larger than that of the least active surface.

To elucidate the role and nature of adsorbed species during the oxidation of ethanol, stripping experiments were performed. In these experiments, the electrode was kept at 0.10 V for 15 minutes in an ethanol containing solution, before being transferred to a clean electrochemical cell without ethanol. In this cell, cyclic voltammograms of the H_{UPD} region were recorded in order to determine the amount and the type of sites blocked directly after adsorption of ethanol on the surface. The resulting voltammograms for Pt (554) are shown in Figure 6.6a. This surface was chosen since it combines an appreciable and well-defined amount of step sites separated by relatively (10 atom) wide terraces. Curve '1' shows the voltammogram of the clean surface before adsorption and shows two distinctive features typical for a stepped surface vicinal to the (111)-direction in an alkaline solution. There is a broad plateau between 0.05 V and 0.35 V, which can be ascribed to hydrogen adsorption/desorption on terrace sites, and a peak at 0.26 V corresponding to (110) step sites. By evaluating these two features individually, it is possible to distinguish between processes occurring at step sites and on terrace sites. Curve '2' was recorded after adsorbing ethanol, which should result in adsorbed single carbon species, $CH_{x,ad}$ and CO_{ad} [9-11]. Comparing to curve '1', it can be clearly seen that the step sites are completely blocked and the terrace sites are partially blocked by the decomposition products. In order to determine the amounts and the preferred adsorption sites of $CH_{x,ad}$ species, the electrode was polarized at 0.0 V for five minutes to reduce all CH_x fragments to methane [10]. After the reductive stripping (curve '3'), it can be seen that the steps are still completely blocked, but all terrace sites are freed. After the reductive stripping, an oxidative stripping sweep

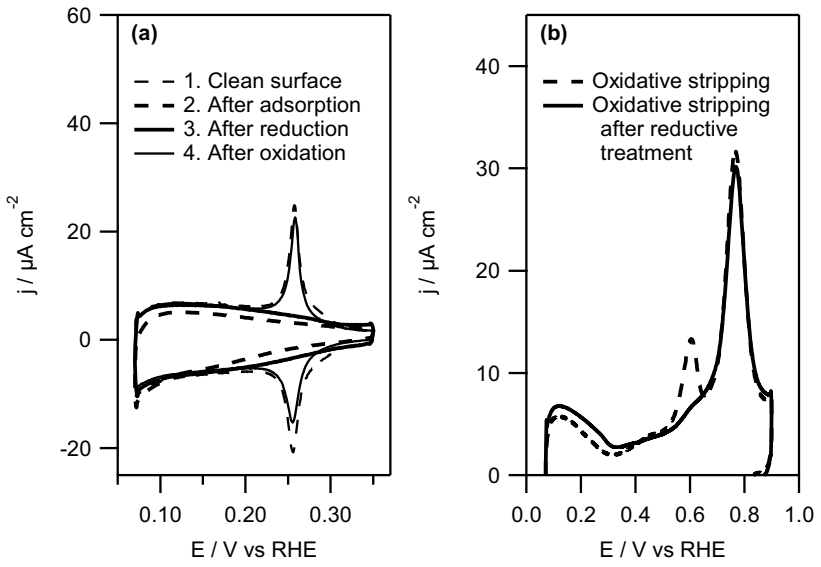

Figure 6.6: *Voltammetric cycles during the stripping experiments on Pt (554) in 0.1 M NaOH. (a) H_{UPD} region as prepared and after various treatments. (b) Comparison of oxidative stripping profile directly after adsorption and preceded by a reductive treatment. The voltammograms are recorded at a sweep rate of 10 mV s^{-1}.*

was performed to remove the remainder of the adsorbed species, which should be mainly CO_{ad}. From the voltammetric profile afterwards (curve '4'), it can be seen that the oxidative sweep liberates the step sites. Finally, it should be noted that the voltammetric profile after the stripping experiment (curve '4') strongly resembles curve '1', suggesting that a clean surface is recovered. Also, since both profiles are similar, there is no indication for (permanent) adsorbate induced surface restructuring, which would surely alter the H_{UPD} region. Alternatively, the oxidative stripping sweep after removing $CH_{x,ad}$ can be compared to an oxidative sweep without a preceding reductive treatment (Figure 6.6b). It can be seen that if a reductive treatment is performed directly after adsorption, the subsequent oxidative stripping curve shows only a single peak around 0.76 V, overlapping with feature for OH_{ad} formation on terrace sites. If, on the other hand, the oxidative stripping curve is not preceded by a reductive treatment, an extra feature appears at 0.60 V [9]. In addition, it takes several voltammetric sweeps (5 - 10) to fully recover the H_{UPD} region in this case.

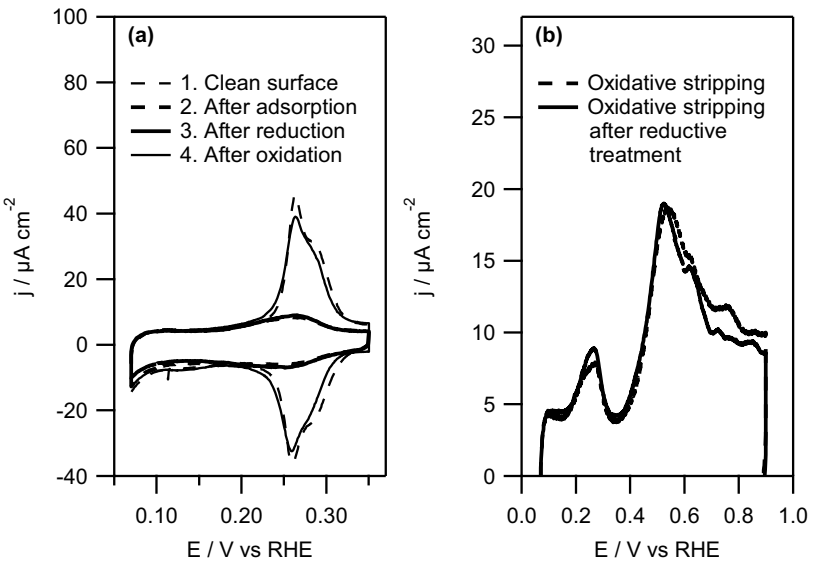

Figure 6.7: *Voltammetric cycles during the stripping experiments on Pt (110) in 0.1 M NaOH. (a) H_{UPD} region as prepared and after various treatments. (b) Comparison of oxidative stripping profile directly after adsorption and preceded by a reductive treatment. The voltammograms are recorded at a sweep rate of 10 mV s^{-1}.*

The findings of these stripping experiments are in good correspondence with the results of similar investigations in acidic media [9] and can be explained as follows. Upon adsorption, ethanol is decomposed and forms adsorbed CH_x (with $x = 1$ in acidic media) and adsorbed CO on the electrode surface. Adsorbed CH_x can be reduced by holding the potential at 0.0 V, fully liberating the terrace sites, leaving the step sites fully blocked by adsorbed CO. Since CO binds stronger to step sites than to terrace sites [45], this suggests that CO is exclusively adsorbed at the step sites, fully blocking it for hydrogen adsorption. The step sites can subsequently be recovered by oxidative stripping of adsorbed CO between 0.7 V and 0.8 V. Interestingly, this potential range corresponds to OH_{ad} formation on terrace sites, suggesting that CO adsorbed on steps is oxidized by OH adsorbed on terraces, in agreement with previous findings [46]. Alternatively, if $CH_{x,ad}$ is not removed by reduction, it can be oxidized to adsorbed CO around 0.6 V before further oxidation to CO_2. Oxidative stripping of $CH_{x,ad}$ however, is somewhat slower, since it takes multiple voltammetric sweeps to recover a

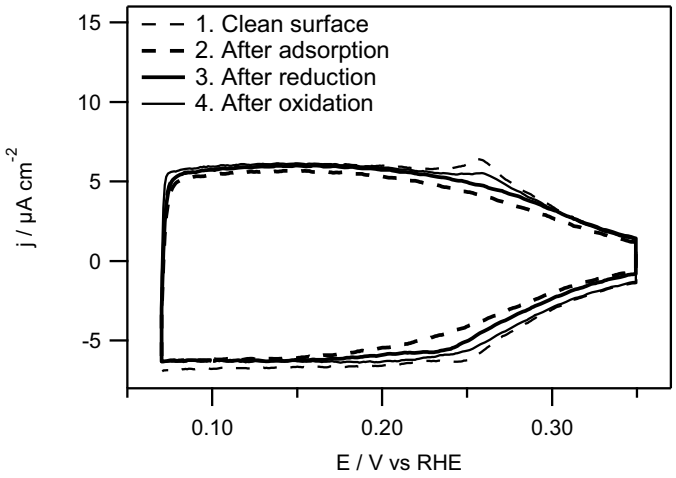

Figure 6.8: *Voltammetric profiles of the H_{UPD} region of Pt (111) in 0.1 M NaOH as prepared and after various treatments during the ethanol adsorbate stripping experiments. The voltammograms are recorded at a sweep rate of 10 mV s^{-1}.*

'clean' H_{UPD} region, whereas adsorbed CO can be stripped within one or two sweeps.

Similar stripping experiments were performed on Pt (110), which lacks terrace sites and showed the highest activity as well as the lowest poisoning rate in the voltammetric experiments. The results of these experiments are shown in Figure 6.7a. On the clean surface, a single feature can be seen in the H_{UPD} region (curve '1'). Similar to Pt (554), ethanol adsorption blocks a significant number of sites for hydrogen adsorption (curve '2'). However, unlike Pt (554), holding the electrode at a reductive potential does not free any sites (curve '3'). Instead, all blocked sites can be liberated by an oxidative stripping sweep (curve '4'). Again, it is clear that the H_{UPD} region shows the same voltammetric profile before and after the stripping experiments, suggesting that no significant permanent surface restructuring has taken place. The oxidative stripping profiles with and without a reductive treatment are shown in Figure 6.7b. Both profiles are virtually identical, demonstrating that a preceding reductive treatment has no significant effect on ethanol adsorbate stripping on Pt (110) in 0.1 M NaOH. These results strongly indicate that no $CH_{x,ad}$ is present on Pt (110).

Finally, the stripping experiments were also performed on Pt (111), which (ideally) consists of infinitely wide terraces (Figure 6.8). As can be seen from the amount of sites blocked for hydrogen adsorption (the difference between curve '1' and curve '2'), ethanol decomposition and subsequent adsorption is relatively slow on Pt (111) compared to Pt (554) and Pt (110). Unlike Pt (554) and Pt (110), however, most sites can be recovered by a reductive stripping treatment (curve '3'), with the subsequent oxidative stripping sweep only liberating a small amount of adsorption sites (curve '4'). Therefore, the combined results for the three surfaces suggest that, in 0.1 M NaOH, $CH_{x,ad}$ species are only stable on (111) terraces.

6.3.2 Surface enhanced Raman spectroscopy

Surface enhanced Raman spectroscopy (SERS) measurements were performed in order to shed more light on the role and the (electro-)chemical nature of the adsorbates. In these measurements, a platinum film deposited on polycrystalline gold was employed as a working electrode. Details on the (electro-)chemical characterization of the electrode in the current set-up can be found in Chapter 5 [5]. In brief, the electrode was prepared by electrochemically roughening a gold electrode followed by depositing a platinum film on top. The thickness of the platinum layer is high enough to mask the (electro-)chemical properties of the bulk underneath, thereby mimicking a bulk platinum electrode, but not too high so as to be able to 'borrow' the SERS enhancement activity from the gold.

In order to be able to correlate the spectroscopic results with the single-crystal electrode experiments, cyclic voltammograms were recorded for the oxidation of ethanol on these platinum film electrodes. The first and twentieth voltammetric cycles are shown in Figure 6.9a. It can be seen that the oxidation of ethanol start at about 0.45 V on the platinum film electrode and that a small hysteresis exists between the anodic and the cathodic sweep. These findings strongly resemble resembles the findings for single-crystal surfaces with a high concentration of low-coordination sites, such as Pt (110) and Pt (553). In addition, the current densities and the deactivation rate (about 50%) found for the platinum film electrodes lie between those found for Pt (110) and Pt (553). The deactivation of platinum film electrode is also illustrated in Figure 6.9b, which shows the current time transients for the platinum film electrode and Pt (110) and Pt (553) for comparison. It can be seen that the current decay over time is qualitatively

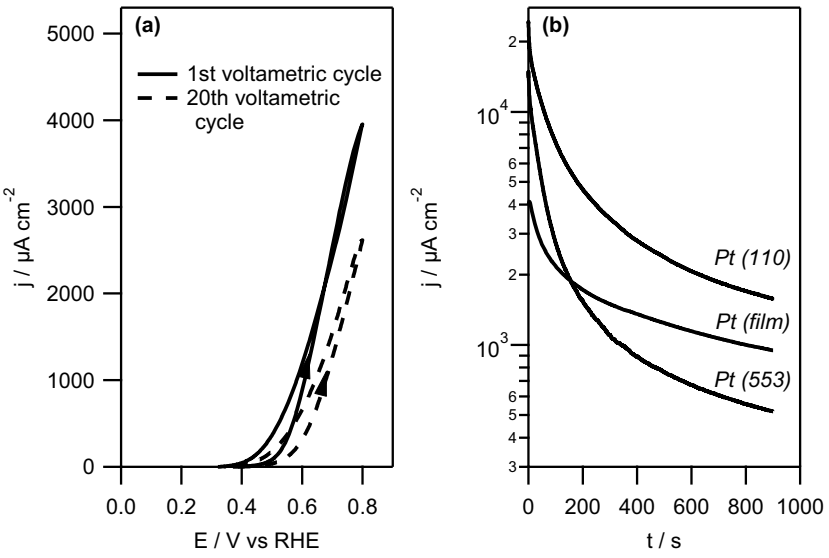

Figure 6.9: *(a) The first and the twentieth voltammetric cycle for the oxidation of 0.5 M ethanol in 0.1 M NaOH on a platinum film deposited on a gold substrate recorded at a sweep rate of 10 mV s^{-1}. (b) Current-time transients for the oxidation of 0.5 M ethanol in 0.1 M NaOH on a platinum film deposited on a gold substrate and on Pt (110). The potential was stepped from 0.07 V to 0.70 V.*

very similar to Pt (110), although the currents are about an order of magnitude lower over the entire time range. After *ca.* 200 s the current density observed for the platinum film electrode lies between that of Pt (553) and Pt (110). These findings strongly indicate that the platinum film electrode has a high concentration of low-coordination sites, with an average concentration between that of Pt (553) and Pt (110). This fact is not surprising since the platinum film electrodes were prepared by electrodepositing platinum on a roughened gold substrate. Therefore, we believe it is meaningful to compare the spectroscopic results on the platinum film electrodes with the electrochemical results of the single-crystal electrodes with a high concentration of low-coordination sites.

For the SERS measurements, ethanol was adsorbed for 15 minutes at 0.10 V before being introduced in the spectroelectrochemical cell, which contained only

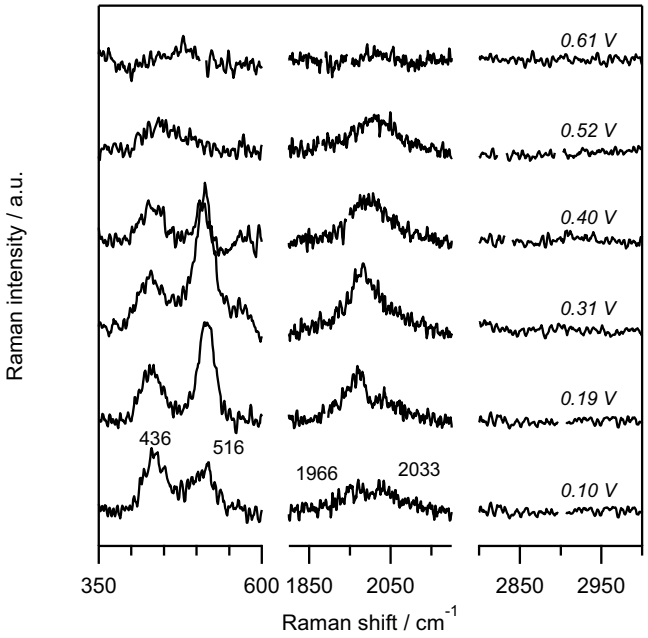

Figure 6.10: *Surface enhanced Raman spectra of adsorbed species coming from ethanol on a Pt-film electrode in 0.1 M NaOH recorded at the indicated potentials.*

supporting electrolyte. The potential was increased in steps of 30 mV and held constant while a SERS spectrum was recorded. A series of typical SERS spectra of ethanolic adsorbates is shown in Figure 6.10. Two spectral regions were found to exhibit significant changes when changing the potential, each containing two adsorption bands. At low wavenumbers, in the region typical for metal-adsorbate vibrations [47], there are signals around 440 cm^{-1} and around 515 cm^{-1}. In addition, there are bands centered on 1960 cm^{-1} and 2035 cm^{-1}. Interestingly, no signals were observed in C-H vibrations region (2800 - 3200 cm^{-1}) [48], suggesting there is no CH_x adsorbed on the electrode surface, nor any other C-H containing adsorbates. In addition to these features, a broad band around 1600 cm^{-1} was observed, corresponding to the bending mode of water [49].

The wavenumber region between 1800 cm^{-1} and 2200 cm^{-1} has been studied extensively with SERS [50, 51] and FTIR [7, 19] and the bands within this region can

be assigned to the intramolecular C-O stretch (ν_{C-O}) of adsorbed CO. More specifically, bands between 2030 cm^{-1} and 2080 cm^{-1} are generally assigned to CO linearly bonded to the platinum surface, while features between 1800 cm^{-1} and 1900 cm^{-1} correspond to bridge-bonded CO. Therefore, the feature at 2035 cm^{-1} can be ascribed unambiguously to CO linearly adsorbed on platinum. In addition, it should be noted that there is a complete absence of a band at *ca.* 2120 cm^{-1}, corresponding to CO adsorbed linearly on residual gold sites [38, 52], further demonstrating the validness of our thin-film approach. The feature at 1960 cm^{-1} cannot be assigned so easily, since its frequency lies just between the regions of bridge-bonded and linearly bonded CO. One possible explanation would be bridge-bonded CO on gold sites, which would be expected around 1950-1970 cm^{-1} [52-54]. However, an adsorption band around 1970 cm^{-1} has also been observed on pure platinum substrates with SERS, FTIR and SFG and has been assigned to bridge-bonded CO [55, 56] or another type of linearly bonded CO [50], presumably on low-coordinated defect-like platinum sites.

In the low wavenumber region, there are two adsorption bands at 440 cm^{-1} and 515 cm^{-1}. This set of double absorption features is well-known for the platinum-carbon stretch of CO adsorbed on platinum [49, 57]. Since the frequency of both bands are too high for CO bonded on gold (260 cm^{-1} and 310 cm^{-1} for adsorption at a bridge site and on top, respectively) [52] and for bridge-bonded CO on platinum (390 cm^{-1}) [38], they may be ascribed to the Pt-C stretch for different types of linearly bonded CO. In addition, the potential dependence of the (relative) intensities of these two bands corresponds well to the intensities of the features in the C-O stretch region. Based on these findings, all features can be assigned to (linearly) adsorbed CO on the platinum film rather than on the gold substrate.

To further substantiate the assignment of the feature at 440 cm^{-1} to adsorbed CO, the same experiments were performed employing deuterated ethanol. The SERS spectra of adsorbates from deuterated ethanol are shown in Figure 6.11. Comparing Figure 6.10 and Figure 6.11, it can clearly be seen that the spectra are virtually identical. Four bands can be observed, similar to the experiments using non-deuterated ethanol. Again, these bands are located around 440 cm^{-1}, 515 cm^{-1}, 1960 cm^{-1} and 2030 cm^{-1}, showing that deuteration does not significantly change the positions of the absorption features. This can be seen more clearly in Figure 6.12, which shows the positions of the SERS features at

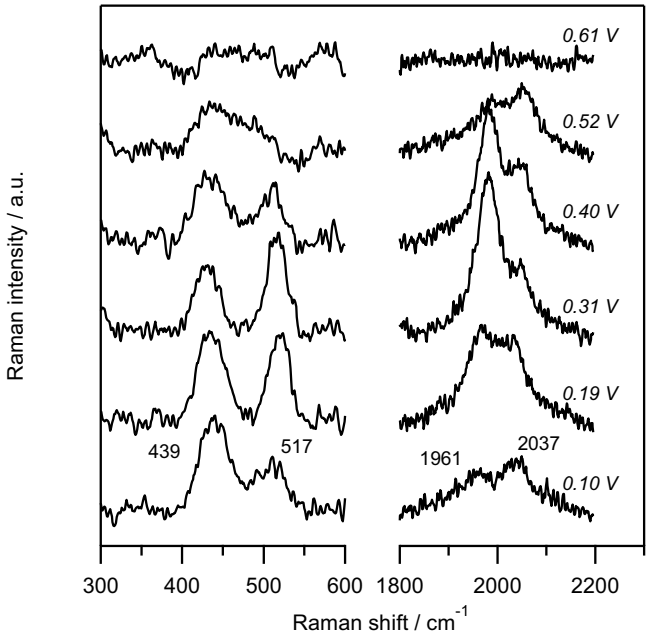

Figure 6.11: *Surface enhanced Raman spectra of adsorbed species coming from deuterated ethanol on a Pt-film electrode in 0.1 M NaOH recorded at the indicated potentials.*

various potentials for CO_{ad} resulting from non-deuterated and deuterated ethanol adsorption. Since exchanging protons for deuterium atoms in $CH_{x,ad}$ or in any hydrogen containing adsorbate would cause a corresponding frequency shift in the SERS band corresponding to the value of x, the lack of a shift of the bands points toward non-hydrogenated adsorbates, supporting CO as the only strongly adsorbed species from the dissociation of ethanol in these experiments.

In addition, it can be seen that CO from both ethanol and deuterated ethanol show the same behavior as a function of potential. At the adsorption potential of 0.10 V, the predominant adsorption state is the state corresponding to 440 cm^{-1} and 2030 cm^{-1} (hereafter denoted as 'I'). Upon initially increasing the potential, the bands at 515 cm^{-1} and 1960 cm^{-1} (hereafter denoted as 'II') gain intensity, while the bands corresponding to adsorption state I slightly lose intensity. This suggests that in the low potential range (up to 0.31 V), there is a conversion

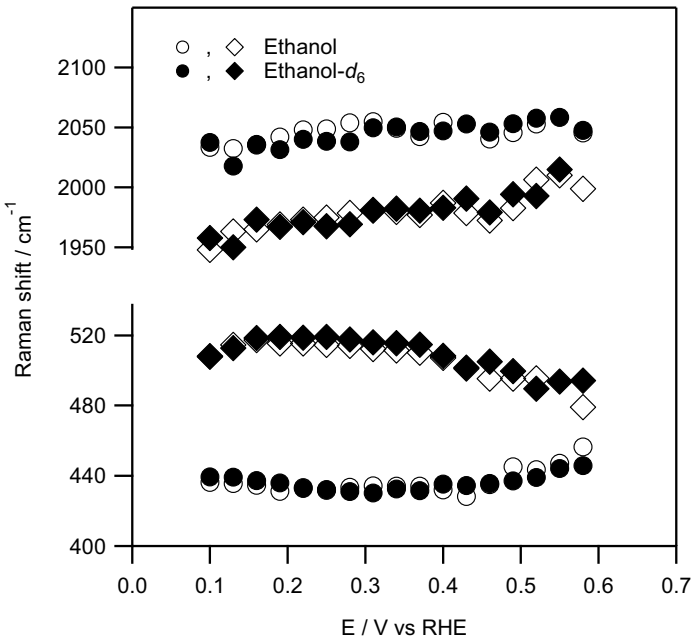

Figure 6.12: *Positions of the SERS bands from CO fragments resulting from ethanol (open symbols) and deuterated ethanol (closed symbols) dissociation.*

from CO in state I, to adsorption state II as the potential is increased. Upon increasing the potential further past 0.31 V, oxidation of CO sets in. Interestingly, it seems that CO adsorbed in state II is the first to be oxidized, while the features associated with state I initially remain relatively constant. Finally, at higher potentials, CO in adsorption state I is also oxidized and a 'clean' surface is recovered. Similar results have also been found in FTIR experiments on CO adlayer oxidation on a 'disordered' Pt (111) electrode in alkaline media, where CO initially adsorbed in a certain state is converted to another adsorption state in which it is more readily oxidized [58].

In conclusion, SERS experiments show that the dissociation of ethanol on a platinum film electrode in a 0.1 M NaOH solution produces only adsorbed CO, which can exist in (at least) two adsorption states, one corresponding to the spectral features at 440 cm^{-1} and 2030 cm^{-1}, and one corresponding to the

features at 515 cm^{-1} and 1960 cm^{-1}. Based on the positions of these features, it is suggested that both states correspond to linear adsorption. The relative stability of these two adsorption states is dependent on the applied potential.

6.4 General discussion

Based on the results described in the previous sections, we can start to build a fundamental understanding of the ethanol electro-oxidation reaction on platinum in an alkaline electrolyte. In addition, we shall compare the findings here with our previous studies in acidic media [5, 9]. It is well-known that the activity for the oxidation of ethanol is greatly enhanced in alkaline media on polycrystalline and nanoparticular surfaces. Similarly, the currents on single-crystal electrodes in alkaline media are significantly larger than those obtained on similar electrodes in acidic media, at least initially. Analogous to acidic media, the initial activity on the single-crystal electrodes is proportional to the amount of step sites, at least at low overpotentials. The effect of step sites, however, is more pronounced in alkaline media. Also, it should be emphasized the onset potential is also strongly dependent on the step density and is as low as 0.35 V for Pt (110), yielding currents which are more than an order of magnitude higher than in an acidic electrolyte at potentials which would be of interest in a direct ethanol fuel cell (*i.e.* below 0.5V). However, all single-crystal surfaces quickly deactivate over time. For surfaces with wide terraces, such as Pt (111) and Pt (15 15 14), the activity drops to less than 10% of the initial activity within twenty voltammetric cycles. Interestingly, the rate of deactivation is also strongly structure sensitive and decreases with decreasing terrace length, suggesting that deactivation is strongly related to terrace sites rather than to step sites.

The stripping experiments indicate that on Pt (554), consisting of 10 atom wide terraces separated by monoatomic (110) steps, two kinds of adsorbates can be found, of which one can be both reduced and oxidized and the other can be only oxidized. Analogous to the adsorbates in acidic media, we propose that the reducible adsorbate is a CH_x species, which can be reduced to form CH_4 [10] or oxidized to adsorbed CO. Similarly, the oxidizable species can be assigned to adsorbed CO, as is also confirmed by the SERS experiments. On Pt (554), CH_x can be found exclusively on terrace sites and CO exclusively on step sites. Also, while CH_x can also be oxidized to adsorbed CO and subsequently to CO_2 (or

CO_3^{2-}), this conversion is slow as it takes multiple (5 - 10) voltammetric sweeps to recover a clean surface, in contrast to acidic media where CH can be oxidatively stripped within one or two voltammetric cycles [9]. Similar results were found for Pt (111). However, the relative amounts of $CH_{x,ad}$ and CO_{ad} differ significantly from Pt (554). By comparing the increase of the charge in the H_{UPD} region due to a reductive treatment to strip $CH_{x,ad}$ with the increase in the charge due to the subsequent oxidative treatment, it is possible to estimate the amounts of $CH_{x,ad}$ and CO_{ad} in terms of sites blocked for hydrogen adsorption. Using this method, it was found that the ratio of sites blocked by $CH_{x,ad}$ species relative to sites blocked by CO_{ad} is 2.0 for Pt (111) and 1.4 for Pt (554), demonstrating that the relative amount of $CH_{x,ad}$ is higher on a surface with a longer terrace length. In contrast, on surfaces with a high concentration of low-coordination sites, such as Pt (110) and the rough platinum film in the SERS experiments, only adsorbed CO is observed. This strongly suggests that $CH_{x,ad}$ in alkaline media is only stable on terrace sites. Since its oxidation is slow, this could explain the high deactivation rate for surfaces with wide terraces.

Based on these findings, we can suggest a detailed model for the oxidation of ethanol on platinum in an aqueous sodium hydroxide solution. Initially, ethanol dissociates at low potentials to form adsorbed CH_x and adsorbed CO. CH_x adsorbed on low-coordination sites is quickly converted into adsorbed CO, while CH_x adsorbed on terrace sites is stable. Based on the SERS results, it can be concluded that there are (at least) two types of linearly adsorbed CO on a surface with a high density of low-coordination sites. Upon increasing the potential, CO_{ad} (which resides on the steps) can be oxidized, while terrace C_1 stripping is slow and incomplete within the time scale of one voltammetric cycle. In the same potential range, ethanol oxidation through the C_2-pathway starts. On surfaces with long terraces, this is the major current producing pathway that occurs mostly on a partially C_1 covered surface, explaining the lack of hysteresis in the voltammetric cycles. On surfaces with shorter terraces, the adsorbates are stripped off more easily causing a bigger hysteresis loop. However, on all surfaces stripping is incomplete within one voltammetric cycle, leading to a buildup of adsorbed species causing deactivation over time. Since the stripping rate is essentially slowed down by increasing terrace length, this readily explains why deactivation is faster for surfaces with wide terraces.

Using this model, we can compare the mechanism of the ethanol oxidation reaction in alkaline media to that in acidic media as we have suggested in the previous chapters [5, 9]. We suggest that the differences in the ethanol oxidation reaction between acidic and alkaline media mainly arise from the different reactivity of adsorbed CH species in alkaline media. In alkaline media, the reactivity of $CH_{x,ad}$ on (110) sites can clearly be distinguished from $CH_{x,ad}$ on (111) terrace sites. On (110) sites, $CH_{x,ad}$ is rapidly oxidized at potentials below 0.10 V to CO_{ad}, while in (111) terrace sites, $CH_{x,ad}$ oxidation does not set in before *ca.* 0.55 V (Figure 6.6). In addition, oxidation on (111) sites is sluggish, since it requires multiple voltammetric cycles to be completely oxidized. In contrast, such a distinction between different surface sites could not be found in acidic media: in all cases $CH_{x,ad}$ was facilely converted to CO around 0.45 V. This strongly suggests that, in alkaline media, (110) sites are the most active in the oxidization of $CH_{x,ad}$ to CO_{ad}, but that CH_x adsorbed on (111) terrace sites are hindered from reaching the active (110) sites, either due to a low surface diffusion rate or because access to these sites is blocked by another adsorbed species. Although it is unclear at the moment why $CH_{x,ad}$ in alkaline media is less stable on (110) sites but more stable on (111) sites compared to acidic media, this observation readily explains the differences in the ethanol oxidation reaction in acidic and alkaline media. As shown in Figure 6.1, the ethanol oxidation reaction on a polycrystalline platinum electrode is significantly increased compared to acidic media. In comparison, the results obtained in the single-crystal electrode experiments show that the current densities obtained in alkaline media on surfaces vicinal to the (111) direction are comparable or even lower than those obtained in acidic media on the same surfaces. Pt (110), on the other hand, shows an enhancement in activity of 1 - 2 orders of magnitude. In addition, the deactivation rate of the reaction in alkaline is also the lowest on Pt (110). Therefore, the enhanced reactivity of polycrystalline electrode in alkaline media mainly stems from the increased activity on low-coordination sites, or, more specifically, on sites with short or no (111) terraces, as these are readily poisoned by $CH_{x,ad}$. This is in stark contrast with acidic media, where the oxidation of CH_{ad} occurs at the same potential regardless of the surface, explaining why the structure sensitivity of the ethanol oxidation reaction is much less pronounced in acidic media.

6.5 Conclusion

In this chapter, we have presented the results of a systematic electrochemical study on the oxidation of ethanol in NaOH solutions. Voltammetric stripping experiments on single-crystal electrodes and SERS experiments on a rough platinum film electrode, show that ethanol adsorption yields adsorbed CO and adsorbed CH_x, similar to the oxidation of ethanol in acidic media. It was found that adsorbed CH_x plays a decisive role in the oxidation of ethanol in an alkaline solution. On (110) sites, $CH_{x,ad}$ is quickly oxidized to CO_{ad}, so that only CO_{ad} is observed on Pt (110) and on the roughened platinum film electrode employed in the SERS experiments. On the other hand, $CH_{x,ad}$ on (111) terrace sites is difficult to oxidize, deactivating the electrode over time. In agreement with this key role of adsorbed CH_x, continuous ethanol oxidation experiments on platinum single-crystal electrodes show a marked dependence of the voltammetric profiles on the surface structure. The onset potential of ethanol oxidation lowers with an increasing density of low-coordination sites. Furthermore, Pt (110) shows the highest oxidation activity for all potentials, both for the initial and long-term activity, while for the surfaces vicinal to (111), the relative dependence of the activity on the step density is potential dependent and changes over time. The deactivation rate was also found to increase with increasing terrace length, which we again attribute to the difficult oxidation of $CH_{x,ad}$ on (111) terrace sites.

6.6 References

1. *Fuel Cell Catalysis: A Surface Science Approach*, M. T. M. Koper (Ed.), John Wiley & Sons, Hoboken, NJ, USA, 2009.
2. S. C. Chang, L. W. H. Leung and M. J. Weaver, *J. Phys. Chem.*, **1990**, *94*, 6013-6021.
3. H. Wang, Z. Jusys and R. J. Behm, *J. Phys. Chem. B*, **2004**, *108*, 19413-19424.
4. G. A. Camara and T. Iwasita, *J. Electroanal. Chem.*, **2005**, *578*, 315-321.
5. S. C. S. Lai, S. E. F. Kleyn, V. Rosca and M. T. M. Koper, *J. Phys. Chem. C*, **2008**, *112*, 19080-19087.

6. J. Shin, W. J. Tornquist, C. Korzeniewski and C. S. Hoaglund, *Surf. Sci.*, **1996**, *364*, 122-130.
7. F. Colmati, G. Tremiliosi-Filho, E. R. Gonzalez, A. Berna, E. Herrero and J. M. Feliu, *Faraday Discuss.*, **2008**, *140*, 379-397.
8. J. F. Gomes, B. Busson and A. Tadjeddine, *J. Phys. Chem. B*, **2006**, *110*, 5508-5514.
9. S. C. S. Lai and M. T. M. Koper, *Faraday Discuss.*, **2008**, *140*, 399-416.
10. U. Schmiemann, U. Muller and H. Baltruschat, *Electrochim. Acta*, **1995**, *40*, 99-107.
11. J. Willsau and J. Heitbaum, *J. Electroanal. Chem.*, **1985**, *194*, 27-35.
12. E. Antolini, *J. Power Sources*, **2007**, *170*, 1-12.
13. C. Lamy, S. Rousseau, E. M. Belgsir, C. Coutanceau and J. M. Léger, *Electrochim. Acta*, **2004**, *49*, 3901-3908.
14. W. J. Zhou, W. Z. Li, S. Q. Song, Z. H. Zhou, L. H. Jiang, G. Q. Sun, Q. Xin, K. Poulianitis, S. Kontou and P. Tsiakaras, *J. Power Sources*, **2004**, *131*, 217-223.
15. H. Wang, Z. Jusys and R. Behm, *J. Appl. Electrochem.*, **2006**, *36*, 1187-1198.
16. S. Sen Gupta and J. Datta, *J. Electroanal. Chem.*, **2006**, *594*, 65-72.
17. F. H. B. Lima and E. R. Gonzalez, *Electrochim. Acta*, **2008**, *53*, 2963-2971.
18. A. Kowal, M. Li, M. Shao, K. Sasaki, M. B. Vukmirovic, J. Zhang, N. S. Marinkovic, P. Liu, A. I. Frenkel and R. R. Adzic, *Nat. Mater.*, **2009**, *8*, 325-330.
19. Q. Wang, G. Q. Sun, L. H. Jiang, Q. Xin, S. G. Sun, Y. X. Jiang, S. P. Chen, Z. Jusys and R. J. Behm, *Phys. Chem. Chem. Phys.*, **2007**, *9*, 2686-2696.
20. A. Wieckowski, J. Sobrowski, P. Zelenay and K. Franaszczuk, *Electrochim. Acta*, **1981**, *26*, 1111-1119.
21. D. M. Dos Anjos, K. B. Kokoh, J. M. Leger, A. R. De Andrade, P. Olivi and G. Tremiliosi, *J. Appl. Electrochem.*, **2006**, *36*, 1391-1397.
22. M. López-Atalaya, E. Morallón, F. Cases, J. L. Vázquez and J. M. Pérez, *J. Power Sources*, **1994**, *52*, 109-117.
23. A. V. Tripkovic, K. D. Popovic and J. D. Lovic, *Electrochim. Acta*, **2001**, *46*, 3163-3173.

24. C. Coutanceau, L. Demarconnay, C. Lamy and J. M. Léger, *J. Power Sources*, **2006**, *156*, 14-19.
25. J. R. Varcoe and R. C. T. Slade, *Electrochem. Commun.*, **2006**, *8*, 839-843.
26. E. R. Choban, L. J. Markoski, A. Wieckowski and P. J. A. Kenis, *J. Power Sources*, **2004**, *128*, 54-60.
27. C. M. Lang, K. Kim and P. A. Kohl, *Electrochem. Solid-State Lett.*, **2006**, *9*, A545-A548.
28. Y. Kiros and S. Schwartz, *J. Power Sources*, **2000**, *87*, 101-105.
29. J. W. Kim and S. M. Park, *J. Electrochem. Soc.*, **2003**, *150*, E560-E566.
30. R. Parsons and T. VanderNoot, *J. Electroanal. Chem.*, **1988**, *257*, 9-45.
31. J. S. Spendelow and A. Wieckowski, *Phys. Chem. Chem. Phys.*, **2007**, *9*, 2654-2675.
32. J. S. Spendelow, G. Q. Lu, P. J. A. Kenis and A. Wieckowski, *J. Electroanal. Chem.*, **2004**, *568*, 215-224.
33. G. García and M. T. M. Koper, *Phys. Chem. Chem. Phys.*, **2008**, *10*, 3802-3811.
34. V. Rao, Hariyanto, C. Cremers and U. Stimming, *Fuel Cells*, **2007**, *7*, 417-423.
35. J. Clavilier, D. Armand, S. G. Sun and M. Petit, *J. Electroanal. Chem.*, **1986**, *205*, 267-277.
36. N. P. Lebedeva, M. T. M. Koper, J. M. Feliu and R. A. van Santen, *Electrochem. Commun.*, **2000**, *2*, 487-490.
37. P. Gao, D. Gosztola, L. W. H. Leung and M. J. Weaver, *J. Electroanal. Chem.*, **1987**, *233*, 211-222.
38. S. Zou and M. J. Weaver, *Anal. Chem.*, **1998**, *70*, 2387-2395.
39. T. Iwasita, X. H. Xia, H. D. Liess and W. Vielstich, *J. Phys. Chem. B*, **1997**, *101*, 7542-7547.
40. J. S. Spendelow, J. D. Goodpaster, P. J. A. Kenis and A. Wieckowski, *J. Phys. Chem. B*, **2006**, *110*, 9545-9555.
41. C. Lamy, J. M. Léger and J. Clavilier, *J. Electroanal. Chem.*, **1982**, *135*, 321-328.
42. J. Clavilier, C. Lamy and J. M. Léger, *J. Electroanal. Chem.*, **1981**, *125*, 249-254.
43. N. M. Markovic and P. N. Ross, *Surf. Sci. Rep.*, **2002**, *45*, 121-229.
44. T. H. M. Housmans and M. T. M. Koper, *J. Phys. Chem. B*, **2003**, *107*, 8557-8567.

45. B. Hammer, O. H. Nielsen and J. K. Nørskov, *Catal. Lett.*, **1997**, *46*, 31-35.
46. G. García and M. T. M. Koper, *J. Am. Chem. Soc.*, **2009**, *131*, 5384-5385.
47. Z. Q. Tian, B. Ren and D. Y. Wu, *J. Phys. Chem. B*, **2002**, *106*, 9463-9483.
48. P. Gao, C. H. Lin, C. Shannon, G. N. Salaita, J. H. White, S. A. Chaffins and A. T. Hubbard, *Langmuir*, **1991**, *7*, 1515-1524.
49. R. Gomez, J. Solla-Gullon, J. M. Perez and A. Aldaz, *J. Raman Spectrosc.*, **2005**, *36*, 613-622.
50. Z. Q. Tian, B. Ren and B. W. Mao, *J. Phys. Chem. B*, **1997**, *101*, 1338-1346.
51. S. Zou and M. J. Weaver, *J. Phys. Chem.*, **1996**, *100*, 4237-4242.
52. G. L. Beltramo, T. E. Shubina and M. T. M. Koper, *ChemPhysChem*, **2005**, *6*, 2597-2606.
53. A. Kudelski and B. Pettinger, *Chem. Phys. Lett.*, **2004**, *383*, 76-79.
54. P. Rodriguez, J. M. Feliu and M. T. M. Koper, *Electrochem. Commun.*, **2009**, *11*, 1105-1108.
55. T. Iwasita, F. C. Nart, B. Lopez and W. Vielstich, *Electrochim. Acta*, **1992**, *37*, 2361-2367.
56. A. Peremans and A. Tadjeddine, *J. Electroanal. Chem.*, **1995**, *395*, 313-316.
57. R. Gomez, J. M. Perez, J. Solla-Gullon, V. Montiel and A. Aldaz, *J. Phys. Chem. B*, **2004**, *108*, 9943-9949.
58. G. García, P. Rodriguez, V. Rosca and M. T. M. Koper, *Langmuir*, **2009**, *25*, 13661-13666..